

Assessing recent trends in high-latitude Southern Hemisphere surface climate

Julie. M. Jones*, Sarah T. Gille, Hugues Goosse, Nerilie J. Abram, Pablo O. Canziani, Dan J. Charman, Kyle R. Clem, Xavier Crosta, Casimir de Lavergne, Ian Eisenman, Matthew H. England, Ryan L. Fogt, Leela M. Frankcombe, Gareth J. Marshall, Valérie Masson-Delmotte, Adele K. Morrison, Anaïs J. Orsi, Marilyn N. Raphael, James A. Renwick, David P. Schneider, Graham R. Simpkins, Eric J. Steig, Barbara Stenni, Didier Swingedouw and Tessa R. Vance.

e-mail: julie.jones@sheffield.ac.uk*

This PDF contains data and methods, supplementary Tables 1-2, and supplementary Figures 1-5.

Data and Methods

Antarctic Climate Monitoring

Figure 1 and Supplementary Figure 2

We used station-based (shaded shapes) and reconstruction-based (shading over Antarctica) temperature data to calculate Antarctic surface air temperature (SAT) trends over the period 1979-2014. Regional SAT was calculated by averaging the station-based temperatures for each respective region denoted by shaded shapes. Only Byrd station is available for West Antarctica; thus only one line is provided for that region. Station-based temperature data are from the quality-controlled SCAR READER (Scientific Committee on Antarctic Research REference Antarctic Data for Environmental Research) Project¹, and the reconstructed data are from the Ohio State University Byrd Polar Research Center's Reconstruction of Antarctic near-surface temperature dataset². Reconstructed temperature data span the period 1979-2012, and trends were scaled to represent the period 1979-2014.

Sea surface temperature (SST) trends (shading over the ocean) were calculated using the National Oceanic and Atmospheric Administration (NOAA) Extended Reconstructed SST version 3b dataset³, employed at 2x2° latitude-longitude resolution. The zonal-mean SST is the average SST over the region 50°S-70°S. Sea ice concentration trends (contours over the ocean) were calculated using the Bootstrap sea ice concentration dataset⁴, which has approximately 25x25 km resolution and which was acquired from the National Snow and Ice Data Center (NSIDC). The regional sea-ice extent (SIE) is the sum of all grid points where ice concentration is greater than 15% in each respective region. The regions used are the entire Antarctic domain (shown in Fig. 1 and supplementary Fig. 2), and the Ross-Amundsen, and Amundsen-Bellingshausen regions (as marked in Fig. 1 and Supplementary Fig. 2). Ten-metre wind data (vectors) are from the ERA-Interim reanalysis dataset⁵ employed at 1°x1° latitude-longitude resolution. The Southern Annular Mode (SAM) is defined using the observation-based Marshall SAM index⁶.

Seasonal means for all metrics are defined with respect to the Southern Hemisphere: austral summer (December-February, DJF), austral autumn (March-May, MAM), austral winter (June-August, JJA), and austral spring (September-November, SON). Annual means are calculated over

January-December. All trends are shown as the total linear trend over 1979-2014 (i.e. annual trend multiplied by 36). The statistical significance of trends (hatching for SST and green vectors for wind) follows a Student's two-tailed t-test with threshold of significance set at the 95% confidence level taking into account autocorrelation by using the effective sample size⁷.

Historical and palaeoclimate data analysis.

Figure 2 and Supplementary Figure 3

A full list of data used for this analysis, including references, is given in supplementary Table 1.

We use observations of SAT from Antarctic stations where long historical observations records exist. We use records beginning in 1959 (immediately following the International Geophysical Year) or earlier. These data are sourced from the READER database maintained by the British Antarctic Survey¹. Temperature information from natural archives comes primarily from the published, publicly available database of the PAGES (Past Global Changes) Antarctic2k working group⁸. The ice core water stable isotope records in this database have been assessed as suitable for high-resolution palaeotemperature reconstructions based on their temporal resolution and age control, and cover the last ~300 to 2000 years of climate history. We also use the Gomez⁹ and Ferrigno¹⁰ ice core isotope records to provide detailed climate information for the southwestern Antarctic Peninsula and a moss bank $\delta^{13}\text{C}$ record¹¹ as an additional palaeotemperature indicator from the northern Antarctic Peninsula. Sea ice indicators were derived from a historical record as well as from chemical records preserved within ice cores that are sensitive to sea ice extent¹² and from diatom assemblage data from marine sediment cores¹³. Diatom assemblages from marine sediment cores also provide indicators of past SST changes. Published temperature change reconstructed through inversion of borehole profiles^{14,15} were also compiled. The locations of these borehole temperature profiles are shown in Supplementary Fig. 4. Note that because of temperature diffusion processes in snow and ice, borehole temperature profiles are unable to preserve signals of multi-decadal temperature fluctuations, and resolution is decreasing with time span.

We assess climate signals over four geographic regions (Fig. 2). These regions group together records with similar signals informed by geographic constraints, cross correlation of records and spatial patterns of sea ice trends in the satellite era. The distribution of records was also taken into account when defining reconstruction regions, and in many cases the scarcity of available records necessitates the regions being very broad. The regions we use are: (1) the Antarctic Peninsula including the Bellingshausen Sea and Scotia Sea/northern Weddell Sea including the South Orkney Islands. It is defined by the region south of 55°S and extending to 65°S between 40°W and 60°W, and to 83°S between 60°W and 100°W. (2) The West Antarctic region covers the West Antarctic Ice Sheet, Ross Ice Shelf and the Amundsen and Ross Seas. It is bounded by the latitudes 55°S to 83°S, and the longitudes 100°W to 163°E. (3) The coastal East Antarctic region spans the margin of East Antarctic from the Victoria Land all the way to the Weddell Sea coast, and the adjacent Indian and Atlantic oceans. It is the region south of 55°S and extending to 72°S between 163°E and 80°E, to 74°S between 80°E and 10°W, and to 83°S between 10°W and 60°W (but excluding the region of the northern Weddell Sea assigned to the Antarctic

Peninsula region). (4) The East Antarctic Plateau region approximately follows the 2000m elevation contour and is defined in this study as being south of 83°S between 10°W and 163°E, south of 72°S between 163°E and 80°E, and south of 74°S between 80°E and 10°W. The assignment of the historical and palaeoclimate records to these regions is shown in Supplementary Table 1.

In order to examine regional climate variability and trends over the past 200 years, all records were first binned as 5-year averages. Where records had less than annual resolution (e.g. marine sediment cores, moss bank), they were resampled as pseudo-annuals using a nearest neighbour interpolation method that distributes the measured value across all years that it represents. This ensures that data are attributed with the correct ratio between adjacent 5-year bins. The 5-year binned records were then converted to anomalies (SAT observations and borehole inversions; °C units) or normalised (proxies for SAT, SST and sea ice; σ units) relative to the mean and standard deviation of data in the bins between 1960 and 1990. This normalization step assumes that temperature-proxy variance is the same in all locations within a region, but the validity of this assumption remains to be assessed. With the exception of borehole temperature records, the 5y binned records were then assigned to their respective geographic region and compiled as 5y averages. These regional compilations are presented in Figure 2.

Trend distributions were assessed for proxy records of SAT, SST and SIE using data at annual average or pseudo-annual resolution (Supplementary Fig. 3). To assess the significance of the most recent 36-year trends we calculate the linear trend across the final 36 years of each proxy record. These trends are comparable in length to the satellite-era trends presented in Fig. 1, but are not the same in timing, as the proxy records end at varying times, and none extend to the end of 2014. These are then compared to the distribution of all other earlier 36-year trends in the proxy record to assess the significance with each proxy record of the most recent 36-year trend. This trend assessment is also repeated using 100-year trends for proxy records that cover at least the past 200 years.

CMIP5 model analysis.

Fig. 3, Supplementary Fig. 5

We selected all CMIP5 models that have a minimum of 250 years' duration in their pre-industrial control simulation and at least one Representative Concentration Pathway 8.5 (RCP8.5) simulation (see Supplementary Table 2 for a list of the 38 models included). Prior to computing the trend distributions shown in Fig. 3, we corrected the modelled sea ice extent, SST, SAT and SAM time series for drift. When we found strong nonlinear drift near the start of pre-industrial simulations, we ignored the corresponding portion of the time series for subsequent analysis. We then calculated a linear trend over the full (remaining) length of pre-industrial control experiments and subtracted it from all time series.

From the detrended pre-industrial time series, we computed 36-year linear trends using a 36-year sliding window with a time step of 1 year. The analysed pre-industrial time series totalled a length of around 20000 years (depending on the variable considered, Supplementary Table 2). The distribution of all 36-year trends were compiled by model and then averaged to produce

the distributions in Figure 3 (Fig. 3a-d, blue), a total of more than 15000 overlapping 36-year trends. To gain an estimate of uncertainty in the trend distributions, we applied a Monte Carlo methodology, whereby this process was repeated 1000 times, but with the individual model distributions based on random selections of 10% of all possible 36-year trends. The 5% and 95% levels across the 1000 replicate multi-model distributions produced were used to estimate uncertainty ranges around the pre-industrial 36-year trend distributions (dark blue error bars in Fig. 3a-d). The same process is repeated for Supplementary Figure 5, but using season-specific model data, and without applying the Monte Carlo uncertainty methodology, as we expect seasonal ranges to be very similar to the annual.

Since available historical experiments generally only cover up to year 2005, years 2006-2014 of RCP8.5 simulations were appended to historical 1979-2005 time series to obtain the modelled distributions of 1979-2014 trends (Fig. 3a-d, black/grey). Scenario forcing RCP8.5 was chosen, because it is the best available match to the observed greenhouse gas emissions trajectory over 2006-2014. Between 1 and 12 historical-RCP8.5 simulations per model were available (Supplementary Table 2), giving a total of 90 sample 1979-2014 trends entering the satellite-era trend distributions. Despite the variable length of preindustrial simulations and the variable number of historical-RCP8.5 members across models, we enforced equal model weights in the ensemble distributions of Fig. 3a-d by normalizing each model's contribution by the corresponding number of available 36-year trends. Note also that 500hPa geopotential height fields were not available for the EC-EARTH model, reducing the total number of 36-year SAM index trends included in the control and 1979-2014 ensemble distributions of Fig. 3d to 3210 and 78, respectively.

The same models and experiments were employed for the trend emergence analysis presented in Fig. 3e-h. For each model and each variable, the 5-95% range of control trend distributions is first evaluated for trend lengths increasing from 36 to 122 years, using all possible trends of that length (i.e. stepped by 1 year). Historical-RCP8.5 trends starting in 1979 are then calculated for each trend length (i.e. 36-year trends represent the 1979-2014 interval; 122-year trends represent the 1979-2100 interval) and each model experiment. The historical-RCP8.5 trends are compared to the statistical distribution of trends of the same length in the corresponding model's control simulation, and we compute the proportion of models where the linear trend in the historical-RCP8.5 interval exceeds the 95% distribution of trends in the pre-industrial control (or falls below the 5% distribution in the case of negative sea ice extent trends). To gain an estimate of uncertainty in trend emergence, we again employ a Monte Carlo process, whereby we replicate this test 1000 times, but assess emergence for each model against a random selection of 10% of all possible trends of the same length in the control simulation of the same model. The 5% and 95% range of emergence profiles across the 1000 replicate emergence tests are shown as the orange bars around the black line in Figure 3e-h. As in Fig. 3a-d, we ensure that models have equal weights in the shown cumulative distributions: for a model with n member experiments, each experiment is given a weight of $1/n$ when calculating the cumulative multi-model trend emergence profile.

Supplementary Tables

Site Name	Record Type	Climate Parameter	Start Year	End Year	Lat. °N	Long. °E	Region	Ref.
Amundsen Scott	Observations	SAT	1957	2014	-90	0	East Antarctic Plateau	1
Casey	Observations	SAT	1959	2014	-66.3	110.5	Coastal East Antarctica	1
Davis	Observations	SAT	1957	2014	-68.6	78	Coastal East Antarctica	1
Dumont d'Urville	Observations	SAT	1956	2014	-66.7	140	Coastal East Antarctica	1
Esperanza	Observations	SAT	1945	2014	-63.4	-57	Antarctic Peninsula	1
Faraday	Observations	SAT	1951	2014	-65.4	-64.4	Antarctic Peninsula	1
Halley	Observations	SAT	1957	2014	-75.5	-26.4	Coastal East Antarctica	1
Mawson	Observations	SAT	1954	2014	-67.6	62.9	Coastal East Antarctica	1
McMurdo	Observations	SAT	1957	2014	-77.9	166.7	West Antarctica	1
Mirny	Observations	SAT	1956	2014	-66.5	90.3	Coastal East Antarctica	1
Orcadas	Observations	SAT	1904	2014	-60.7	-44.7	Antarctic Peninsula	1
Syowa	Observations	SAT	1957	2014	-69	39.6	Coastal East Antarctica	1
Vostok	Observations	SAT	1958	2014	-78.5	106.9	East Antarctic Plateau	1
Byrd	Observations	SAT	1957	2013	-80	-119.4	West Antarctica	16
Talos Dome	Ice core water isotopes	SAT	1232	1995	-72.5	159.1	East Antarctic Plateau	8,17
Law Dome DSS	Ice core water isotopes	SAT	174	2007	-66.8	112.8	Coastal East Antarctica	8,18
Plateau Remote	Ice core water isotopes	SAT	2	1986	-84	43	East Antarctic Plateau	8,19,20

Site Name	Record Type	Climate Parameter	Start Year	End Year	Lat. °N	Long. °E	Region	Ref.
IND-22 B4	Ice core water isotopes	SAT	1533	1994	-70.9	11.5	Coastal East Antarctica	8,21,22
EDML	Ice core water isotopes	SAT	166	1996	-75	0	East Antarctic Plateau	23, 8
WAIS 2005A	Ice core water isotopes	SAT	743	2005	-79.5	-112.1	West Antarctica	24,8
ITASE 00-1	Ice core water isotopes	SAT	1674	2000	-79.4	-111.2	West Antarctica	24,8,25
ITASE 00-5	Ice core water isotopes	SAT	1719	2000	-77.7	-124.0	West Antarctica	8,24,25
Siple Station	Ice core water isotopes	SAT	1417	1983	-75.9	-84.3	Antarctic Peninsula	8,25,26
JRI	Ice core water isotopes	SAT	0	2007	-64.2	-57.7	Antarctic Peninsula	27,28
Gomez	Ice core water isotopes	SAT	1857	2005	-73.6	-70.4	Antarctic Peninsula	9
Ferrigno	Ice core water isotopes	SAT	1703	2010	-74.6	-86.9	Antarctic Peninsula	10
Lazarav Bay	Moss bank $\delta^{13}\text{C}$	SAT	1863	2003	-69.4	-71.8	Antarctic Peninsula	11
WAIS Divide	Borehole temperature	SAT	8	2007	-79.5	-112.1	West Antarctica	14
Larissa	Borehole temperature	SAT	1810	2007	-66	-64	Antarctic Peninsula	29
DML NUS0702	Borehole temperature	SAT	1509	2008	-76.1	22.5	East Antarctic Plateau	30
DML NUS0705	Borehole temperature	SAT	1509	2008	-78.7	35.6	East Antarctic Plateau	30
DML NUS0707	Borehole temperature	SAT	1509	2008	-82.1	54.9	East Antarctic Plateau	30
DML NUS0805	Borehole temperature	SAT	1509	2009	-82.6	17.9	East Antarctic Plateau	30
Mill Island	Borehole temperature	SAT	1921	2011	-65.6	100.8	Coastal East Antarctica	31

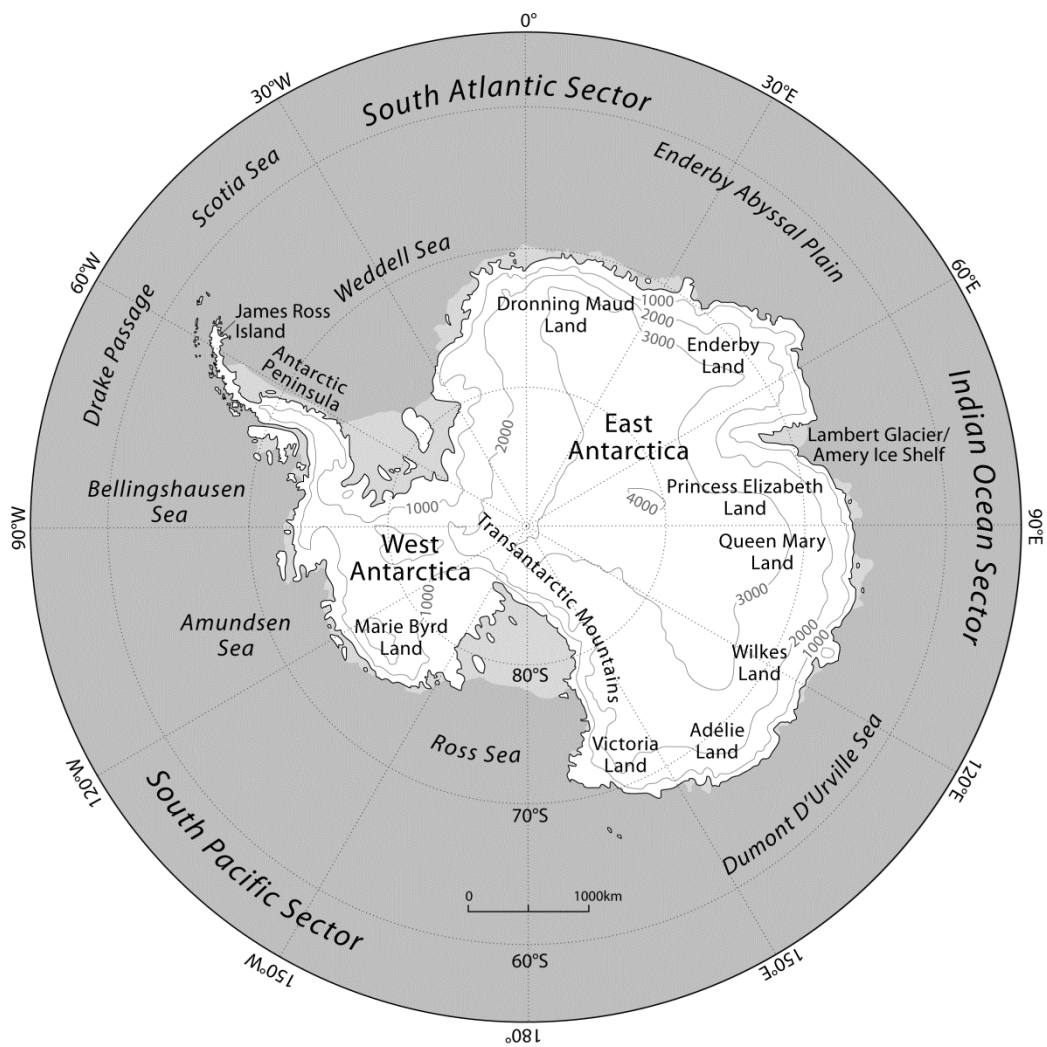
Site Name	Record Type	Climate Parameter	Start Year	End Year	Lat. °N	Long. °E	Region	Ref.
Rutford	Borehole temperature	SAT	1700	2005	-78.1	-83.9	Antarctic Peninsula	32
MCT18a	Diatom assemblage	SST	1864	1999	-64.7	-62.8	Antarctic Peninsula	13
MCT38c	Diatom assemblage	SST	1916	2000	-64.7	-57.4	Antarctic Peninsula	13
CB2010	Diatom assemblage	SST	1740	2001	-66.9	142.4	Coastal East Antarctica	33
West Peninsula stack	Ice core MSA	Winter SIE	1902	1990	-71.9	-74.6	Antarctic Peninsula	34
Law Dome	Ice core MSA	Winter SIE	1841	1995	-66.8	112.8	Coastal East Antarctica	35
South Orkney Fast Ice	Observations	winter SIE	1903	2008	-60.7	-44.7	Antarctic Peninsula	36
MCT18a	Diatom assemblage	SI duration	1864	1999	-64.7	-62.8	Antarctic Peninsula	13
MCT38c	Diatom assemblage	SI duration	1916	2000	-64.7	-57.4	Antarctic Peninsula	13
CB2010	Diatom assemblage	SI duration	1740	2001	-66.9	142.4	Coastal East Antarctica	33

Supplementary Table 1: Details of the long observational records and palaeoclimate proxy records used in this study (Fig. 2, Supplementary Fig. 3)

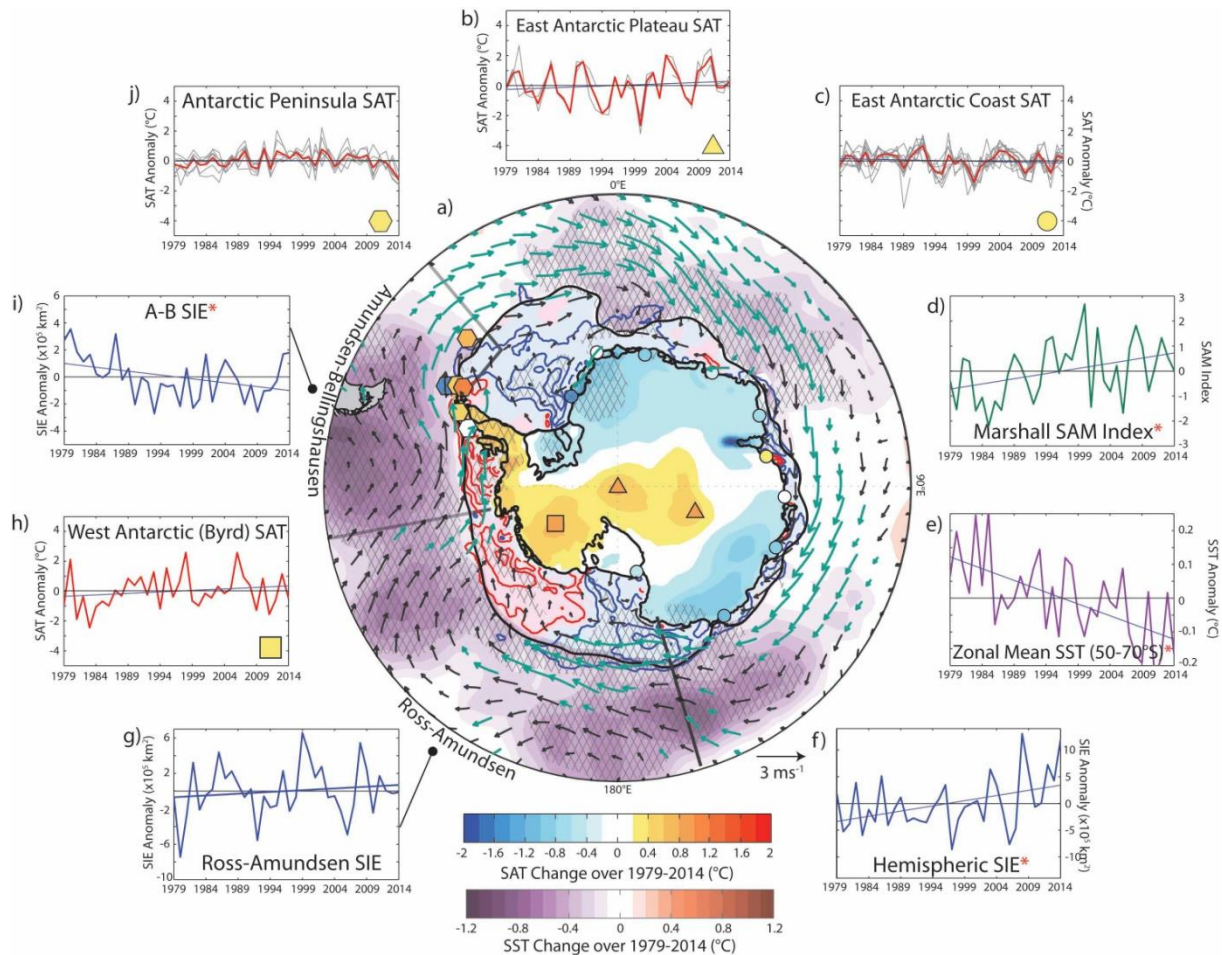
Model	Analysed pre-industrial control length (years)	Number of historical-RCP8.5 member simulations
ACCESS1.0	500	1
ACCESS1.3	500	1
BCC-CSM1.1	500	1
BCC-CSM1.1m	400	1
BNU-ESM	550	1
CanESM2	1096	5
CCSM4	1051	6
CESM1-BGC	500	1
CESM1-CAM5	319	3
CMCC-CESM	276	1
CMCC-CM	330	1
CMCC-CMS	500	1
CNRM-CM5	850	5
CSIRO-Mk3.6	500	10
EC-EARTH	452	12
FGOALS-g2	700	1
FGOALS-s2	501	3
FIO-ESM	800	3
GFDL-CM3	500	1
GFDL-ESM2G	500	1
GFDL-ESM2M	500	1
GISS-E2-H	540	1
GISS-E2-H-CC	250	1
GISS-E2-R	550	2
GISS-E2-R-CC	250	1
HadGEM2-ES	340	4
INM-CM4	500	1
IPSL-CM5A-LR	1000	4
IPSL-CM5A-MR	300	1
IPSL-CM5B-LR	300	1
MIROC-ESM	630	1
MIROC-ESM-CHEM	254	1
MIROC5	700	5
MPI-ESM-LR	1000	3
MPI-ESM-MR	1000	1
MRI-CGCM3	630	1
NorESM1-M	601	1
NorESM1-ME	252	1
Total number of 36-year trends	~19000	90

Supplementary Table 2: CMIP5 experiments included in the analysis. The length of pre-industrial control experiments after removal of years characterized by nonlinear drift are indicated for each of the 38 selected models, along with the number of available historical-RCP8.5 members. Note that the SAM index could not be computed for the EC-EARTH model, reducing the total number of 36-year trends entering preindustrial and 1979-2014 ensemble distributions.

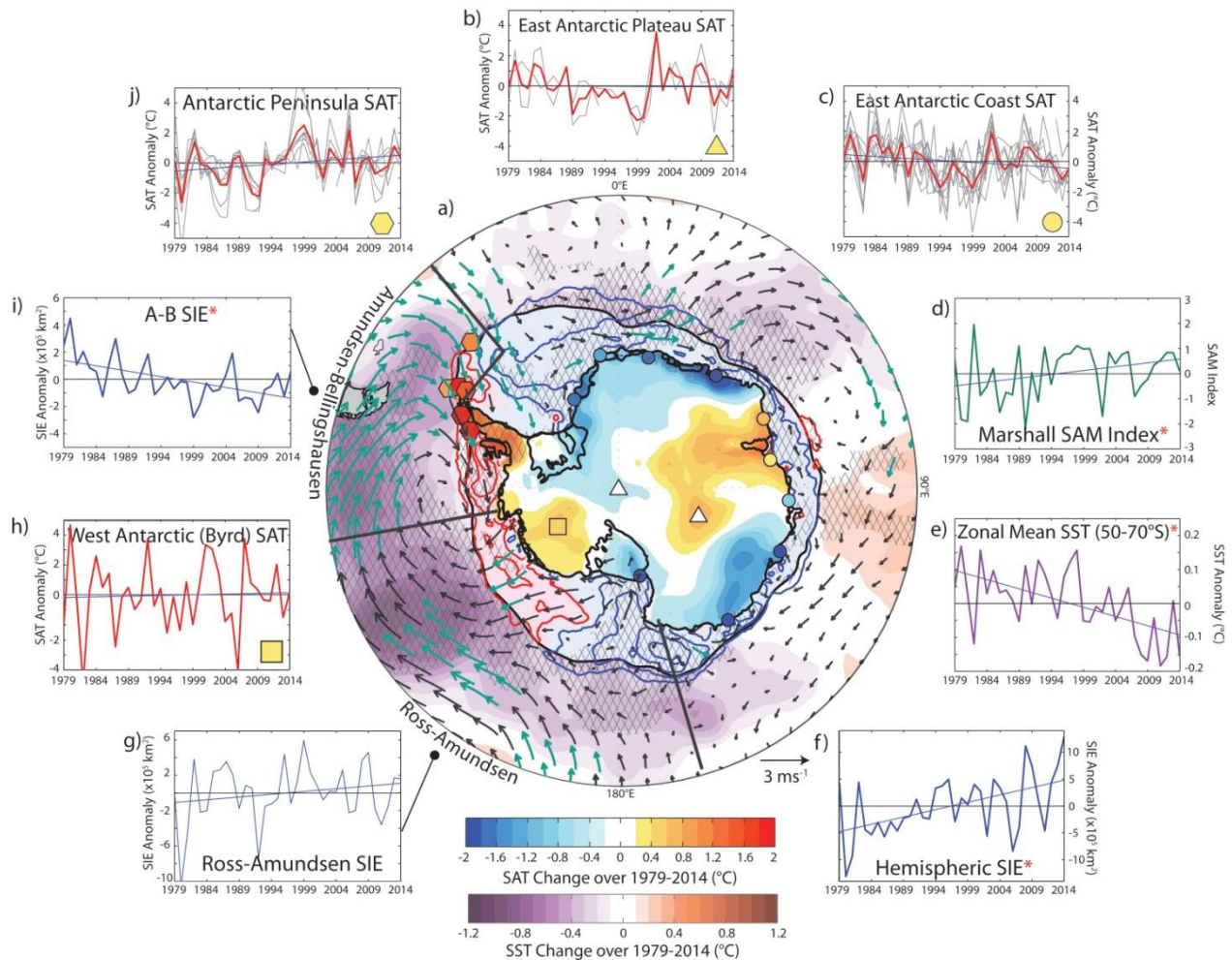
Supplementary Figures



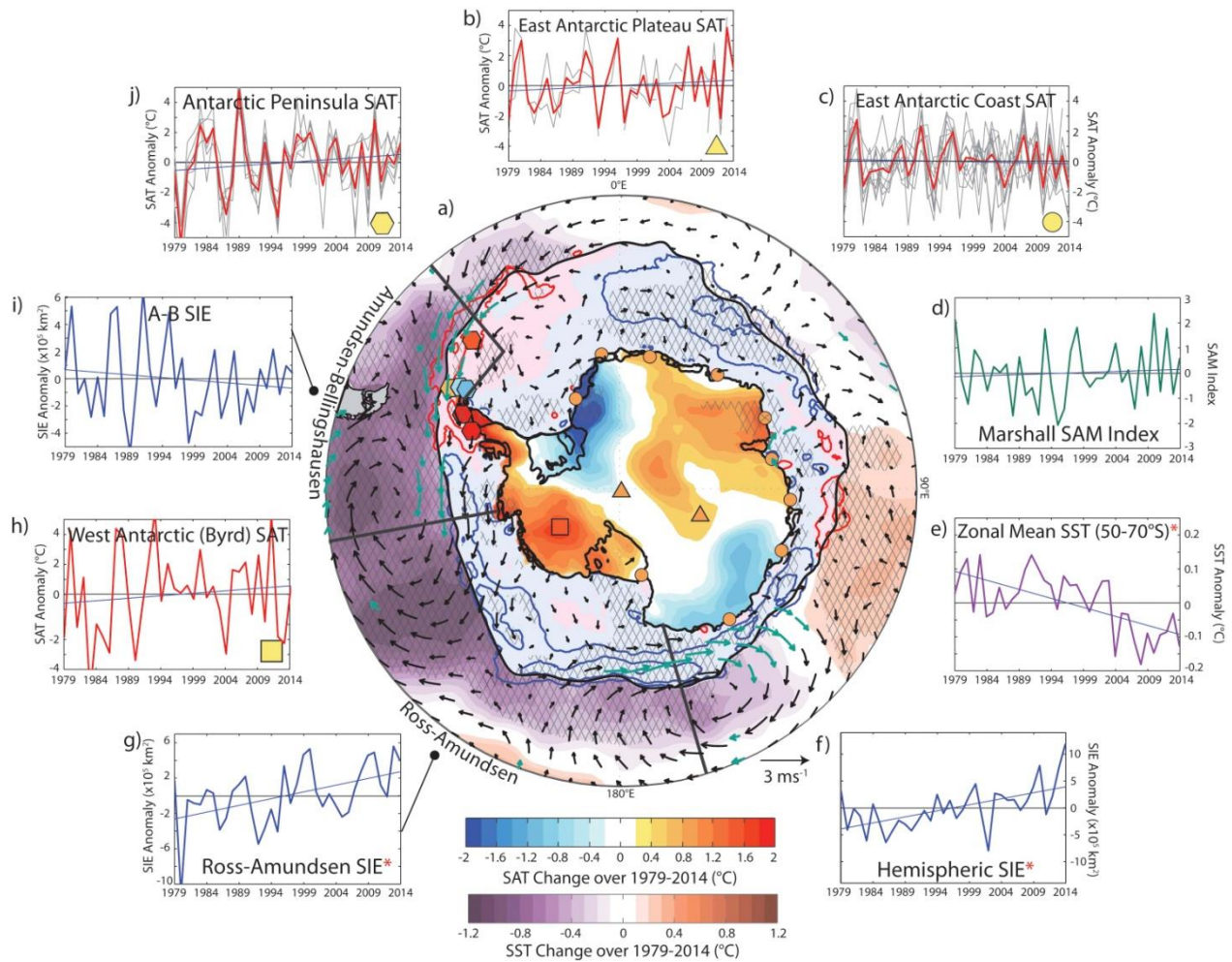
Supplementary Figure 1: Map of the high latitude Southern Hemisphere, including place names mentioned in the text.



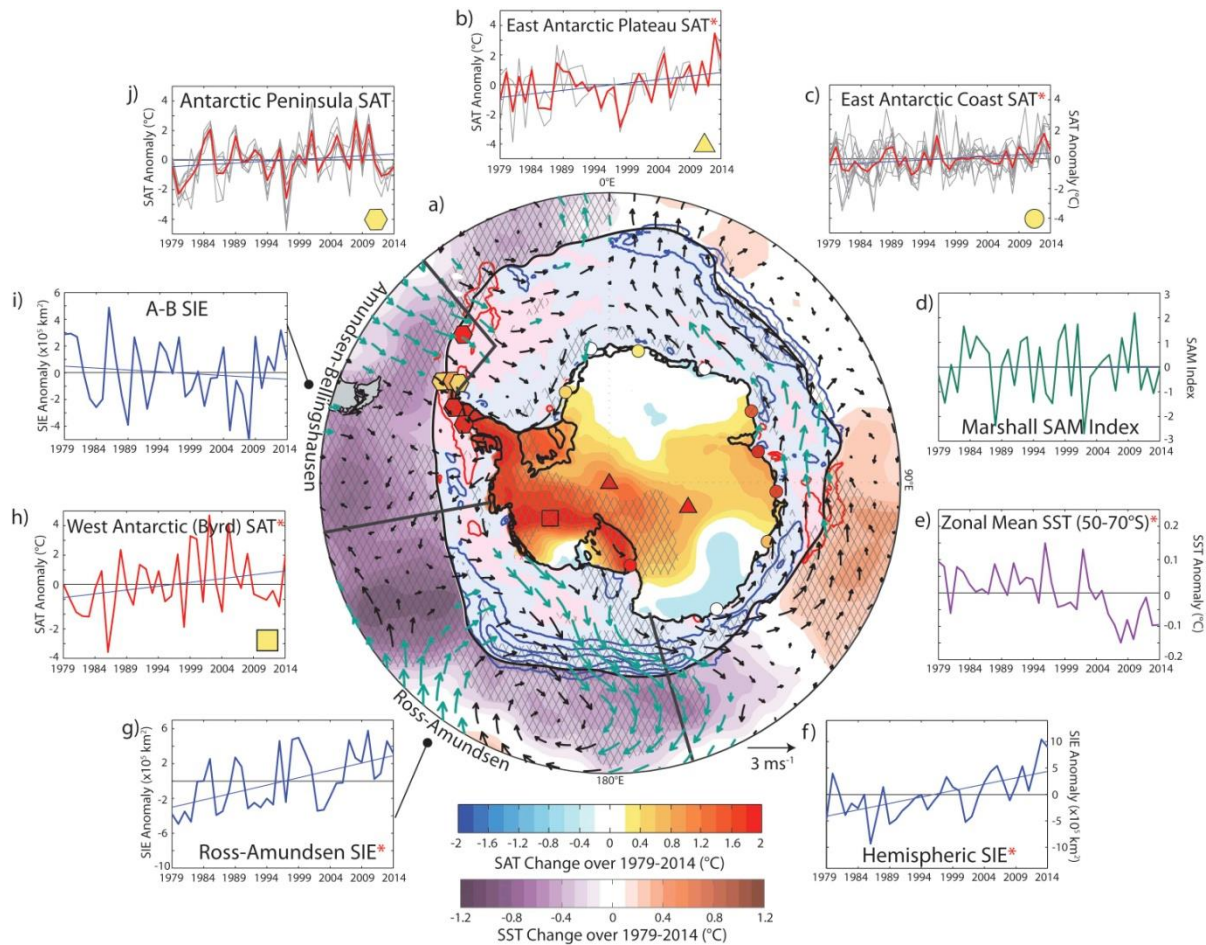
Supplementary Figure 2 a: Antarctic atmosphere-ocean-ice changes over the satellite-observing era for Summer (December, January, February). **a)** Total changes over 1979-2014 in remote sensing annual mean SAT (blue-red shading), station-based SAT (blue-red shaded shapes), sea ice concentration (contours, 10% intervals; red and blue contours, alongside light pink and blue shading beneath, denote negative and positive trends, respectively), SST (purple-red shading), and 10m winds (vectors). Remote sensing SST trends are only shown for areas equatorward of the climatological September SIE (black contour). Hatching and teal vectors highlight trends significant at the 95% level according to two-tailed student t-tests. Note that SAT trends are calculated over 1979-2012 but scaled to represent trends over the 36-year period, 1979-2014. Surrounding figures show time-series of **b)** East Antarctic SAT (circles; red line denotes multi-station mean, grey lines those of individual East Antarctic stations), **c)** the Marshall Southern Annular Mode index (difference in station sea level pressure between 40 and 65°S), **d)** Southern Ocean zonal mean SST (averaged over 50°–70°S), **e)** Southern Hemisphere SIE, **f)** Ross-Amundsen SIE, **g)** West Antarctic SAT (square; Byrd Station), **h)** Amundsen-Bellingshausen SIE, and **i)** Antarctic Peninsula SAT (hexagons; red line denotes multi-station mean, grey lines those of individual Antarctic Peninsula stations). For all time series, blue lines highlight the linear trend, and red asterisks highlight trends that pass a 95% significance two-tailed student t-test. See methods for details on datasets and trend significance calculation.



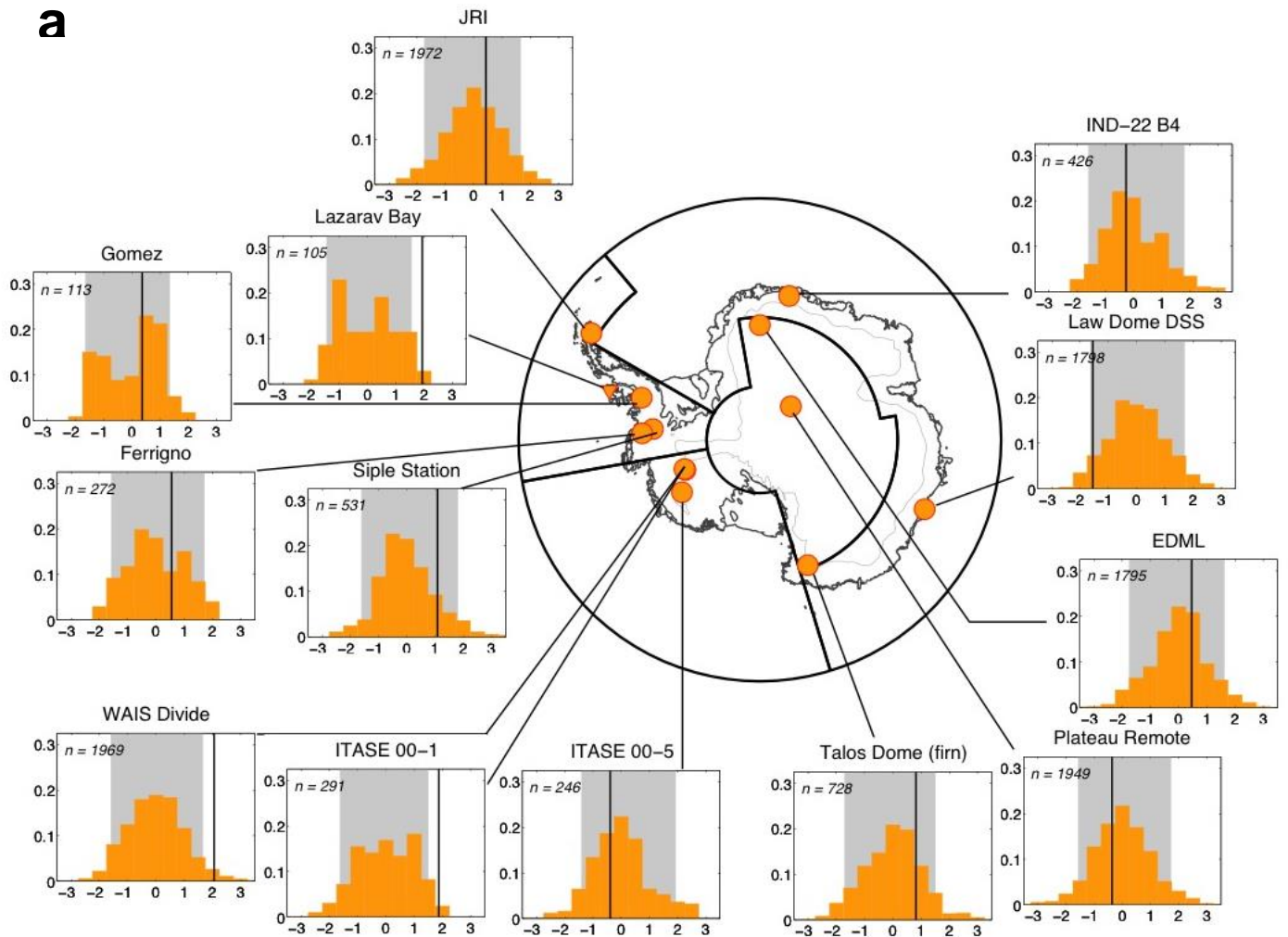
Supplementary Figure 2b: Antarctic atmosphere-ocean-ice changes over the satellite-observing era for Autumn (March, April, May). **a)** Total changes over 1979-2014 in remote sensing annual mean SAT (blue-red shading), station-based SAT (blue-red shaded shapes), sea ice concentration (contours, 10% intervals; red and blue contours, alongside light pink and blue shading beneath, denote negative and positive trends, respectively), sea surface temperature (purple-red shading), and 10m winds (vectors). Remote sensing SST trends are only shown for areas equatorward of the climatological September SIE (black contour). Hatching and teal vectors highlight trends significant at the 95% level according to two-tailed student t-tests. Note that SAT trends are calculated over 1979-2012 but scaled to represent trends over the 36-year period, 1979-2014. Surrounding figures show time-series of **b)** East Antarctic SAT (circles; red line denotes multi-station mean, grey lines those of individual East Antarctic stations), **c)** the Marshall Southern Annular Mode index (difference in station sea level pressure between 40 and 65°S), **d)** Southern Ocean zonal mean SST (averaged over 50°–70°S), **e)** Southern Hemisphere SIE, **f)** Ross-Amundsen SIE, **g)** West Antarctic SAT (square; Byrd Station), **h)** Amundsen-Bellinghshausen SIE, and **i)** Antarctic Peninsula SAT (hexagons; red line denotes multi-station mean, grey lines those of individual Antarctic Peninsula stations). For all time series, blue lines highlight the linear trend, and red asterisks highlight trends that pass a 95% significance two-tailed student t-test. See methods for details on datasets and trend significance calculation.



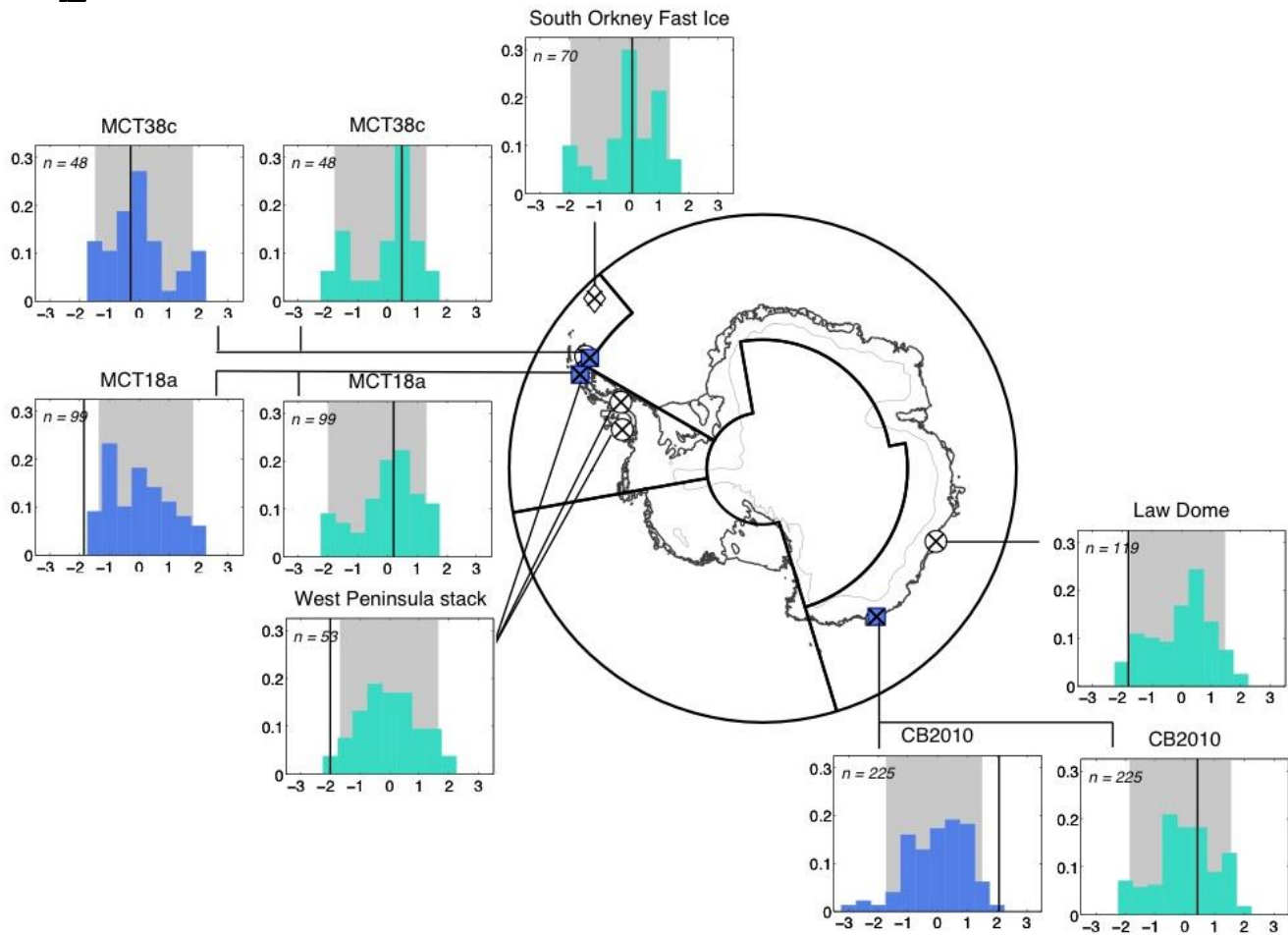
Supplementary Figure 2c: Antarctic atmosphere-ocean-ice changes over the satellite-observing era for Winter (June, July, August). **a)** Total changes over 1979–2014 in remote sensing annual mean SAT (blue-red shading), station-based SAT (blue-red shaded shapes), sea ice concentration (contours, 10% intervals; red and blue contours, alongside light pink and blue shading beneath, denote negative and positive trends, respectively), sea surface temperature (purple-red shading), and 10m winds (vectors). Remote sensing SST trends are only shown for areas equatorward of the climatological September SIE (black contour). Hatching and teal vectors highlight trends significant at the 95% level according to two-tailed student t-tests. Note that SAT trends are calculated over 1979–2012 but scaled to represent trends over the 36-year period, 1979–2014. Surrounding figures show time-series of **b)** East Antarctic SAT (circles; red line denotes multi-station mean, grey lines those of individual East Antarctic stations), **c)** the Marshall Southern Annular Mode index (difference in station sea level pressure between 40 and 65°S), **d)** Southern Ocean zonal mean SST (averaged over 50°–70°S), **e)** Southern Hemisphere SIE, **f)** Ross-Amundsen SIE, **g)** West Antarctic SAT (square; Byrd Station), **h)** Amundsen-Bellingshausen SIE, and **i)** Antarctic Peninsula SAT (hexagons; red line denotes multi-station mean, grey lines those of individual Antarctic Peninsula stations). For all time series, blue lines highlight the linear trend, and red asterisks highlight trends that pass a 95% significance two-tailed student t-test. See methods for details on datasets and trend significance calculation.



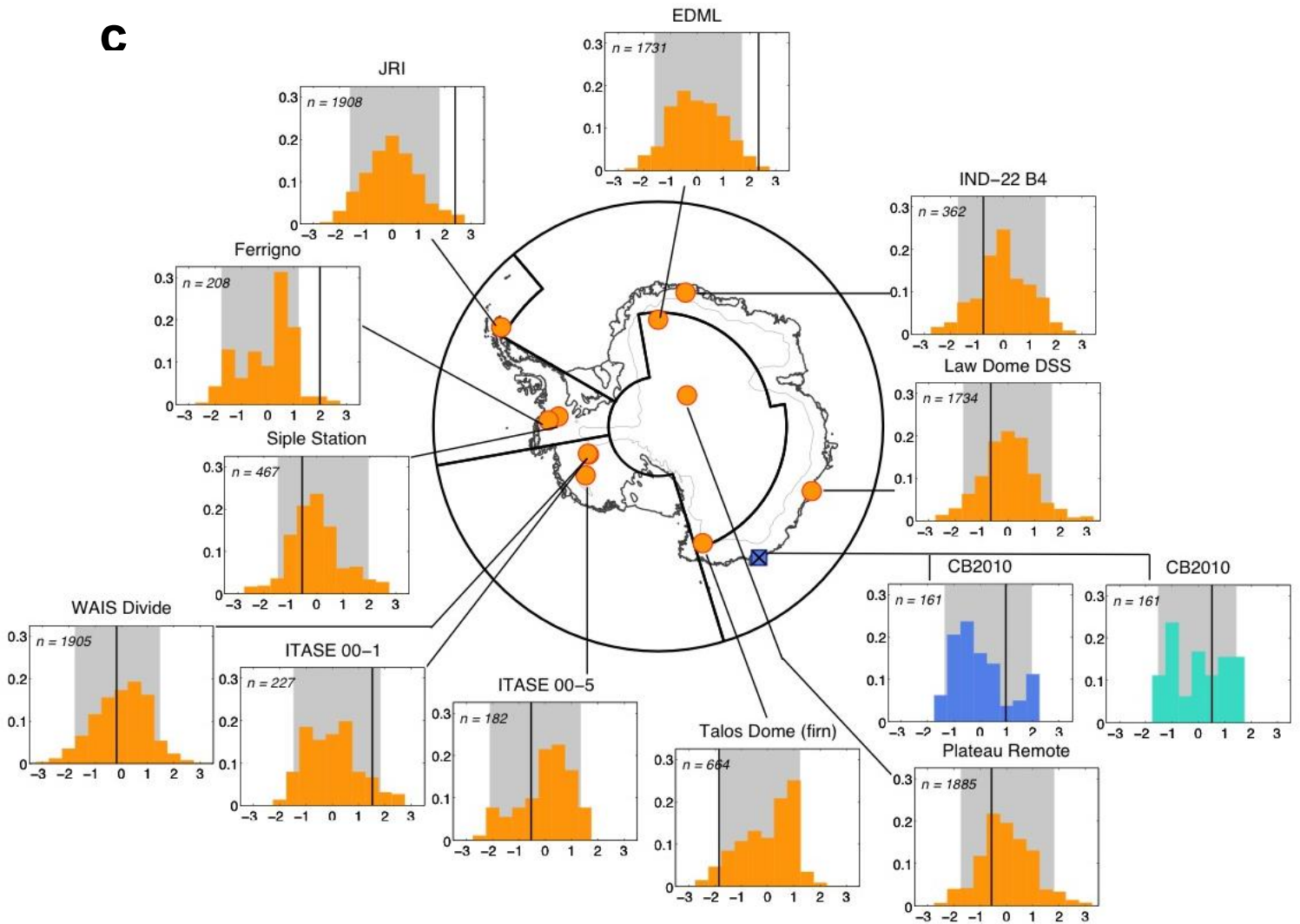
Supplementary Figure 2d: Antarctic atmosphere-ocean-ice changes over the satellite-observing era for Spring (September, October, November). **a)** Total changes over 1979-2014 in remote sensing annual mean SAT (blue-red shading), station-based SAT (blue-red shaded shapes), sea ice concentration (contours, 10% intervals; red and blue contours, alongside light pink and blue shading beneath, denote negative and positive trends, respectively), sea surface temperature (purple-red shading), and 10m winds (vectors). Remote sensing SST trends are only shown for areas equatorward of the climatological September SIE (black contour). Hatching and teal vectors highlight trends significant at the 95% level according to two-tailed student t-tests. Note that SAT trends are calculated over 1979-2012 but scaled to represent trends over the 36-year period, 1979-2014. Surrounding figures show time-series of **b)** East Antarctic SAT (circles; red line denotes multi-station mean, grey lines those of individual East Antarctic stations), **c)** the Marshall Southern Annular Mode index (difference in station sea level pressure between 40 and 65°S), **d)** Southern Ocean zonal mean SST (averaged over 50°–70°S), **e)** Southern Hemisphere SIE, **f)** Ross-Amundsen SIE, **g)** West Antarctic SAT (square; Byrd Station), **h)** Amundsen-Bellinghshausen SIE, and **i)** Antarctic Peninsula SAT (hexagons; red line denotes multi-station mean, grey lines those of individual Antarctic Peninsula stations). For all time series, blue lines highlight the linear trend, and red asterisks highlight trends that pass a 95% significance two-tailed student t-test. See methods for details on datasets and trend significance calculation.

a

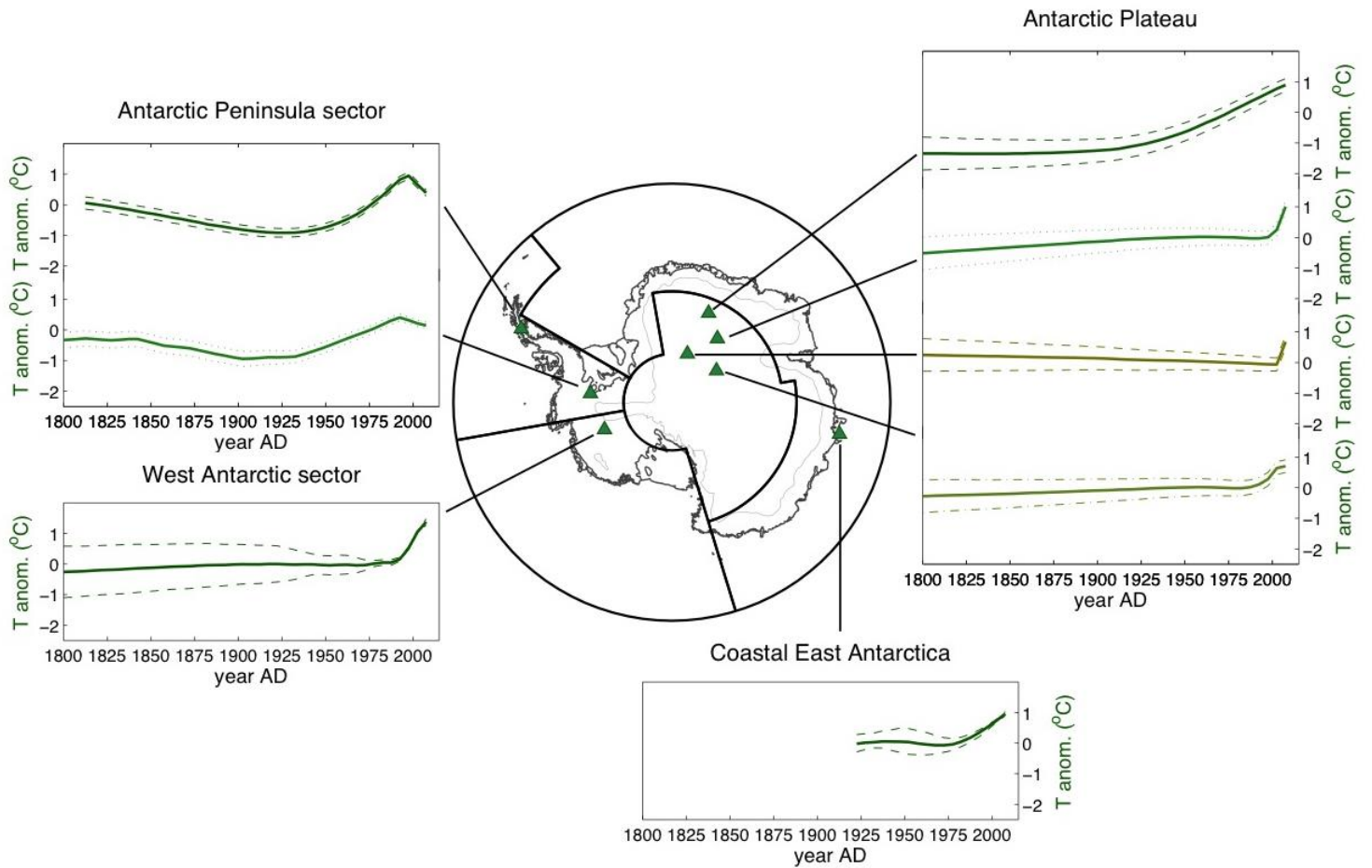
Supplementary Figure 3 (a-c): Significance of recent trends in paleoclimate records. (a) Comparison of the most recent 36y linear trend (black vertical line) in SAT proxy records, compared with all other 36y linear trends in the same SAT proxy record (orange histograms). Grey shading shows the 5-95% range of all 36y trends and n-values denote the total number of 36y trends, excluding the most recent trend. To aid visualisation, the x-axes for all histograms are in normalised trend units (calculated across all trends for a record), and trend occurrence (y-axis) is expressed as a proportion of the total number of trends (n). (b) As in (a) but for SST (blue) and sea ice (cyan) proxy records. (c) As in (a-b) but with trend analysis based on 100y linear trends and shown for SAT (orange), SST (blue) and sea ice (cyan) proxies where records are at least 200 years long.

b

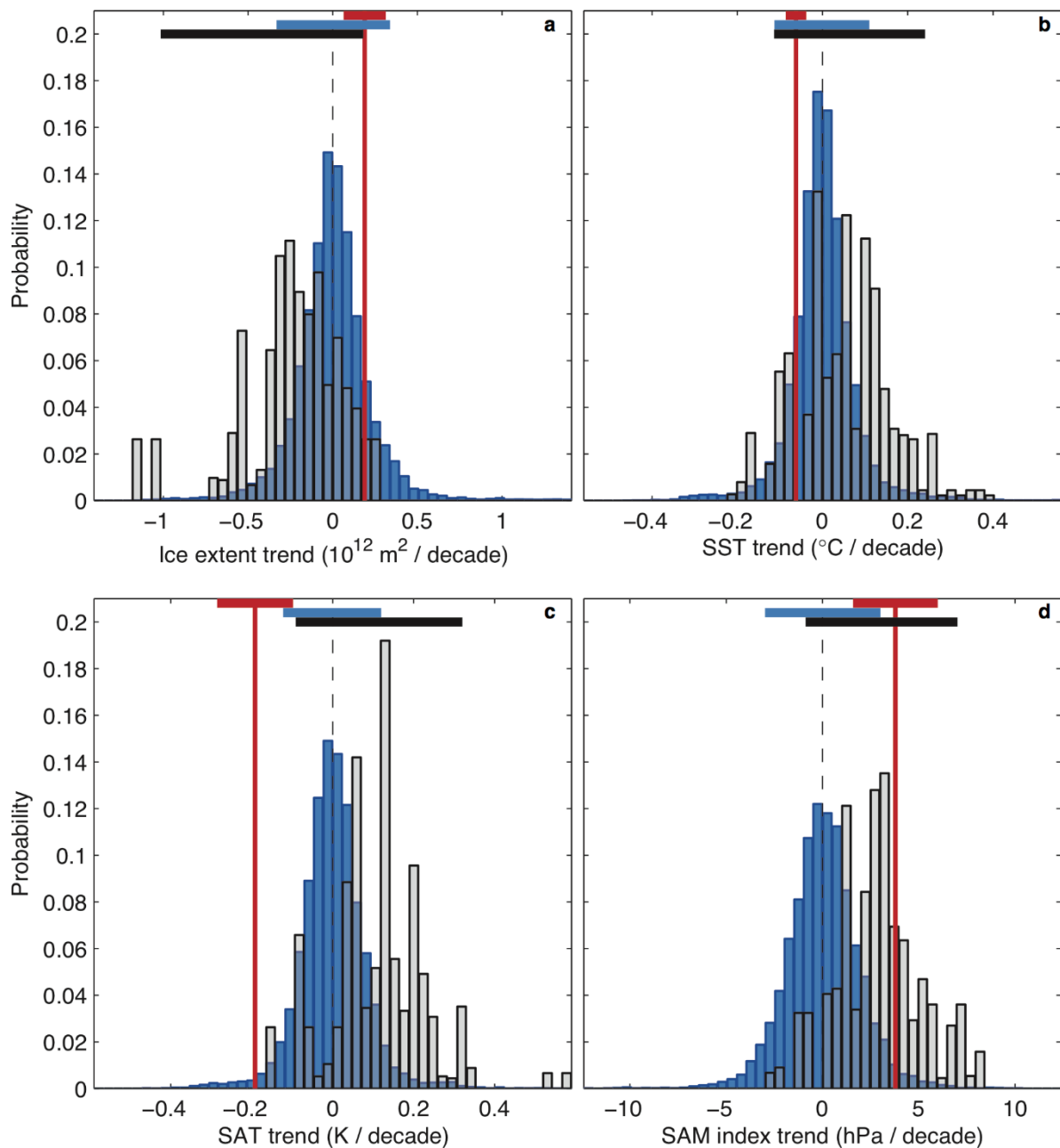
Supplementary Figure 3 (a-c) continued: Significance of recent trends in paleoclimate records. (a) Comparison of the most recent 36y linear trend (black vertical line) in SAT proxy records, compared with all other 36y linear trends in the same SAT proxy record (orange histograms). Grey shading shows the 5-95% range of all 36y trends and n-values denote the total number of 36y trends, excluding the most recent trend. To aid visualisation the x-axes for all histograms are in normalised trend units (calculated across all trends for a record) and trend occurrence (y-axis) is expressed as a proportion of the total number of trends (n). (b) As in (a) but for SST (blue) and sea ice (cyan) proxy records. (c) As in (a-b) but with trend analysis based on 100y linear trends and shown for SAT (orange), SST (blue) and sea ice (cyan) proxies where records are at least 200 years long.



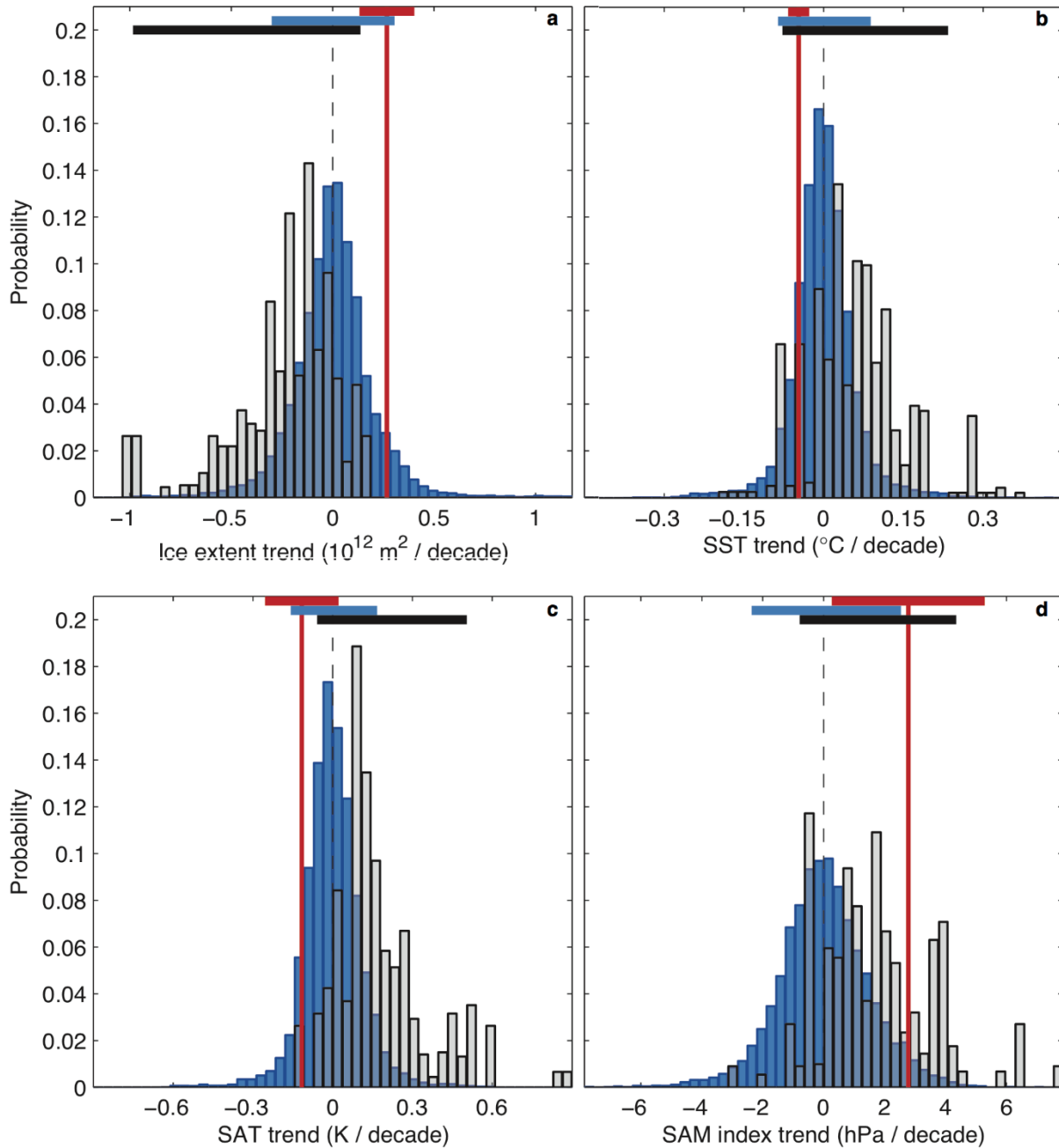
Supplementary Figure 3 (a-c) continued: Significance of recent trends in paleoclimate records. (a) Comparison of the most recent 36y linear trend (black vertical line) in SAT proxy records, compared with all other 36y linear trends in the same SAT proxy record (orange histograms). Grey shading shows the 5-95% range of all 36y trends and n-values denote the total number of 36y trends, excluding the most recent trend. To aid visualisation the x-axes for all histograms are in normalised trend units (calculated across all trends for a record) and trend occurrence (y-axis) is expressed as a proportion of the total number of trends (n). (b) As in (a) but for SST (blue) and sea ice (cyan) proxy records. (c) As in (a-b) but with trend analysis based on 100y linear trends and shown for SAT (orange), SST (blue) and sea ice (cyan) proxies where records are at least 200 years long.



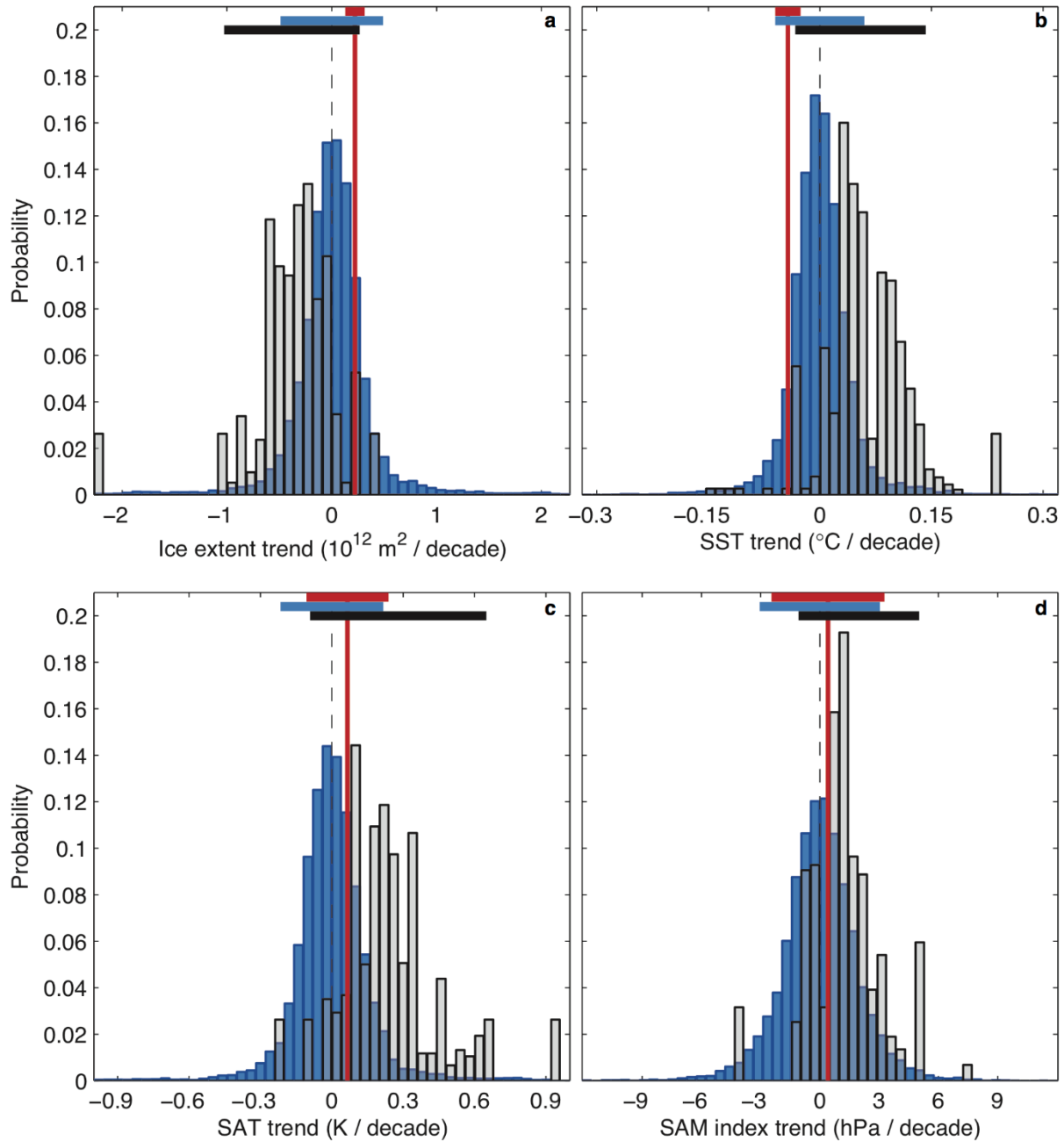
Supplementary Figure 4: Antarctic borehole temperature inversion records. Individual borehole temperature inversions (solid lines) are shown along with their uncertainty bounds (dashed/dotted lines). Colours for each record correspond to those used in Figure 2, but are shown here so that the location of each borehole temperature inversion record can be identified. Details of the individual records provided in Supplementary Table 1.



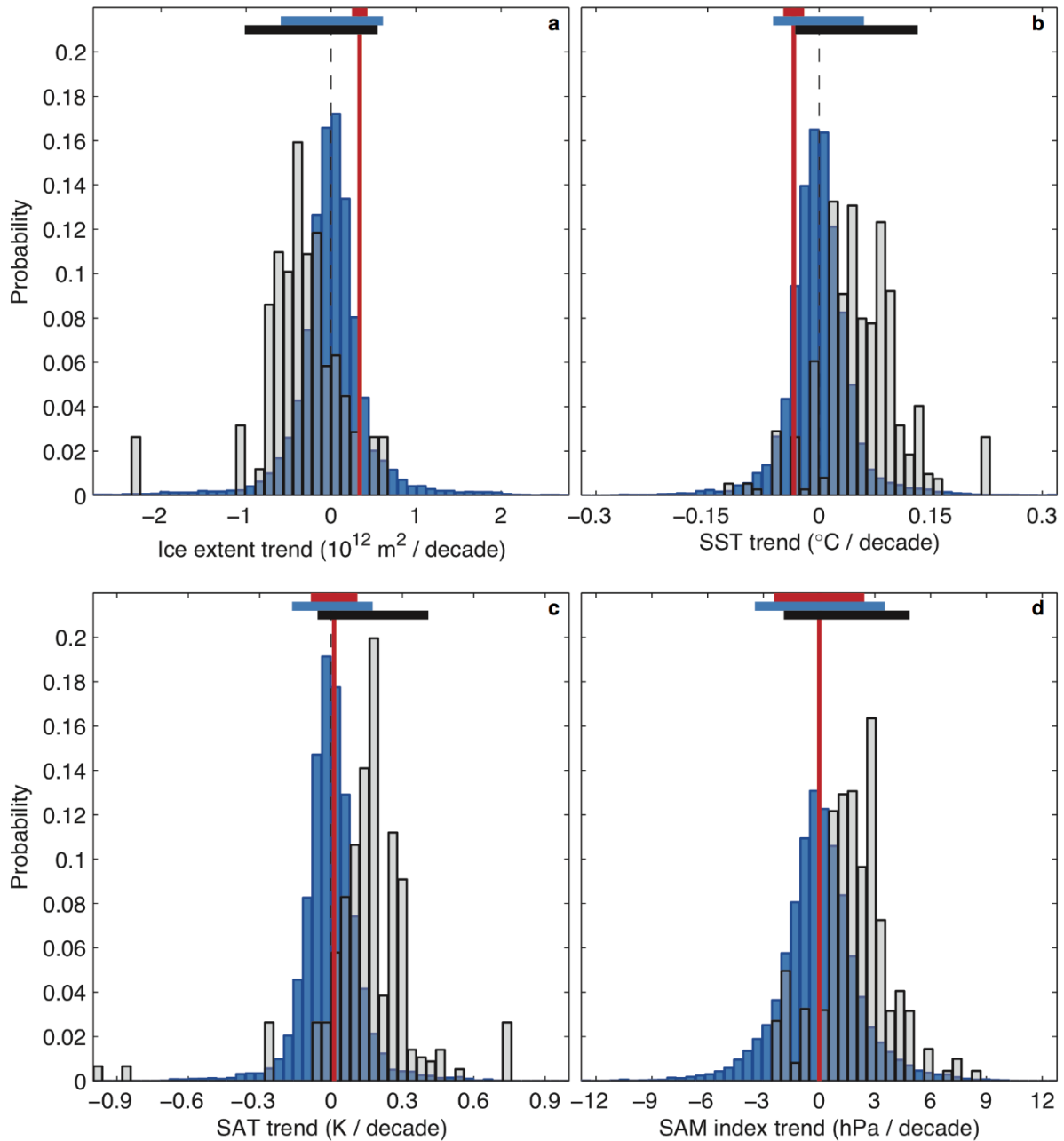
Supplementary Figure 5 DJF: CMIP5 ensemble distributions of 36-year summer (DJF) linear trends in (blue) the ensemble of preindustrial simulations and (black/grey) the ensemble of 1979-2014 historical-RCP8.5 simulations. Panels show **(a)** Southern Hemisphere sea-ice extent, **(b)** mean SST south of 50°S , **(c)** mean SAT south of 50°S and **(d)** SAM index. The red vertical lines correspond to the recent observed 36-year linear trends (1979-2014). Horizontal bars depict (red) the 90% confidence interval of the observed trend, (blue) the 5-95% range of the preindustrial distribution and (black) the 5-95% range of the 1979-2014 trend distribution. Trend calculation methods and data sources are identical to those of Fig. 3a-d.



Supplementary Figure 5 MAM: CMIP5 ensemble distributions of 36-year autumn (MAM) linear trends in (blue) the ensemble of preindustrial simulations and (black/grey) the ensemble of 1979-2014 historical-RCP8.5 simulations. Panels show **(a)** Southern Hemisphere sea-ice extent, **(b)** mean SST south of 50°S, **(c)** mean SAT south of 50°S and **(d)** SAM index. The red vertical lines correspond to the recent observed 36-year linear trends (1979-2014). Horizontal bars depict (red) the 90% confidence interval of the observed trend, (blue) the 5-95% range of the preindustrial distribution and (black) the 5-95% range of the 1979-2014 trend distribution. Trend calculation methods and data sources are identical to those of Fig. 3a-d.



Supplementary Figure 5 JJA: CMIP5 ensemble distributions of 36-year winter (JJA) linear trends in (blue) the ensemble of preindustrial simulations and (black/grey) the ensemble of 1979-2014 historical-RCP8.5 simulations. Panels show **(a)** Southern Hemisphere sea-ice extent, **(b)** mean SST south of 50°S , **(c)** mean SAT south of 50°S and **(d)** SAM index. The red vertical lines correspond to the recent observed 36-year linear trends (1979-2014). Horizontal bars depict (red) the 90% confidence interval of the observed trend, (blue) the 5-95% range of the preindustrial distribution and (black) the 5-95% range of the 1979-2014 trend distribution. Trend calculation methods and data sources are identical to those of Fig. 3a-d.



Supplementary Figure 5 SON: CMIP5 ensemble distributions of 36-year spring (SON) linear trends in (blue) the ensemble of preindustrial simulations and (black/grey) the ensemble of 1979-2014 historical-RCP8.5 simulations. Panels show **(a)** Southern Hemisphere sea-ice extent, **(b)** mean SST south of 50°S , **(c)** mean SAT south of 50°S and **(d)** SAM index. The red vertical lines correspond to the recent observed 36-year linear trends (1979-2014). Horizontal bars depict (red) the 90% confidence interval of the observed trend, (blue) the 5-95% range of the preindustrial distribution and (black) the 5-95% range of the 1979-2014 trend distribution. Trend calculation methods and data sources are identical to those of Fig. 3a-d.

References

- 1 Turner, J. *et al.* The SCAR READER project: Toward a high-quality database of mean Antarctic meteorological observations. *Journal of Climate* **17**, 2890-2898, doi:10.1175/1520-0442(2004).
- 2 Nicolas, J. P. & Bromwich, D. H. New Reconstruction of Antarctic Near-Surface Temperatures: Multidecadal Trends and Reliability of Global Reanalyses. *Journal of Climate* **27**, 8070-8093, doi:10.1175/jcli-d-13-00733.1 (2014).
- 3 Smith, T. M., Reynolds, R. W., Peterson, T. C. & Lawrimore, J. Improvements to NOAA's historical merged land-ocean surface temperature analysis (1880-2006). *Journal of Climate* **21**, 2283-2296, doi:10.1175/2007jcli2100.1 (2008).
- 4 Comiso, J. C. Bootstrap Sea Ice Concentrations from Nimbus-7 SMMR and DMSP SSM/I-SSMIS, Version 2 [NSIDC-0-79]. National Snow and Ice Data Center Distributed Active, Boulder, Colorado, doi: <http://dx.doi.org/10.5067/J6JQLS9EJ5HU>. (2000, 2015 update).
- 5 Dee, D. P. *et al.* The ERA-Interim reanalysis: configuration and performance of the data assimilation system. *Quarterly Journal of the Royal Meteorological Society* **137**, 553-597, doi:10.1002/qj.828 (2011).
- 6 Marshall, G. J. Trends in the southern annular mode from observations and reanalyses. *Journal of Climate* **16**, 4134-4143, doi:10.1175/1520-0442 (2003).
- 7 Santer, B. D. *et al.* Statistical significance of trends and trend differences in layer-average atmospheric temperature time series. *Journal of Geophysical Research-Atmospheres* **105**, 7337-7356, doi:10.1029/1999jd901105 (2000).
- 8 PAGES 2K Consortium. Continental-scale temperature variability during the past two millennia. *Nature Geoscience* **6**, 339-346, doi:10.1038/ngeo1797 (2013).
- 9 Thomas, E. R., Marshall, G. J. & McConnell, J. R. A doubling in snow accumulation in the western Antarctic Peninsula since 1850. *Geophysical Research Letters* **35**, doi:10.1029/2007gl032529 (2008).
- 10 Thomas, E. R., Bracegirdle, T. J., Turner, J. & Wolff, E. W. A 308 year record of climate variability in West Antarctica. *Geophysical Research Letters* **40**, 5492-5496, doi:10.1002/2013gl057782 (2013).
- 11 Royles, J. *et al.* Plants and Soil Microbes Respond to Recent Warming on the Antarctic Peninsula. *Current Biology* **23**, 1702-1706, doi:10.1016/j.cub.2013.07.011 (2013).
- 12 Abram, N. J., Wolff, E. W. & Curran, M. A. J. A review of sea ice proxy information from polar ice cores. *Quaternary Science Reviews* **79**, 168-183, doi:10.1016/j.quascirev.2013.01.011 (2013).
- 13 Barbara, L., Crosta, X., Schmidt, S. & Masse, G. Diatoms and biomarkers evidence for major changes in sea ice conditions prior the instrumental period in Antarctic Peninsula. *Quaternary Science Reviews* **79**, 99-110, doi:10.1016/j.quascirev.2013.07.021 (2013).
- 14 Orsi, A. J., Cornuelle, B. D. & Severinghaus, J. P. Little Ice Age cold interval in West Antarctica: Evidence from borehole temperature at the West Antarctic Ice Sheet (WAIS) Divide. *Geophysical Research Letters* **39**, doi:10.1029/2012gl051260 (2012).

- 15 Clow, G. D. The extent of temporal smearing in surface-temperature histories derived from borehole temperature measurements. *Palaeogeography Palaeoclimatology Palaeoecology* **98**, 81-86, doi:10.1016/0031-0182(92)90189-c (1992).
- 16 Bromwich, D. H. *et al.* Central West Antarctica among the most rapidly warming regions on Earth. *Nature Geoscience* **6**, 139-145, doi:10.1038/ngeo1671 (2013).
- 17 Stenni, B. *et al.* Eight centuries of volcanic signal and climate change at Talos Dome (East Antarctica). *Journal of Geophysical Research-Atmospheres* **107**, doi:10.1029/2000jd000317 (2002).
- 18 Plummer, C. T. *et al.* An independently dated 2000-yr volcanic record from Law Dome, East Antarctica, including a new perspective on the dating of the 1450s CE eruption of Kuwae, Vanuatu. *Climate of the Past* **8**, 1929-1940, doi:10.5194/cp-8-1929-2012 (2012).
- 19 Cole-Dai, J. H., Mosley-Thompson, E., Wight, S. P. & Thompson, L. G. A 4100-year record of explosive volcanism from an East Antarctica ice core. *Journal of Geophysical Research-Atmospheres* **105**, 24431-24441, doi:10.1029/2000jd900254 (2000).
- 20 Mosley-Thompson, E. Holocene Climate Changes Recoded in an East Antarctica Ice Core, in *Climatic Variations and Forcing Mechanisms of the Last 2000 years* (eds P. D Jones, R. S. Bradley, & J. Jouzel) 263-269 (Springer-Verlag, 1996).
- 21 Thamban, M. *et al.* Aerosol perturbations related to volcanic eruptions during the past few centuries as recorded in an ice core from the Central Dronning Maud Land, Antarctica. *Current Science* **91**, 1200-1207 (2006).
- 22 Laluraj, C. M. *et al.* Nitrate records of a shallow ice core from East Antarctica: Atmospheric processes, preservation and climatic implications. *Holocene* **21**, 351-356, doi:10.1177/0959683610374886 (2011).
- 23 Graf, W. *et al.* Stable-isotope records from Dronning Maud Land, Antarctica. Supplement to *Annals of Glaciology*, 35, 195-201, doi:10.1594/PANGAEA.104862 (2002).
- 24 Steig, E. J. *et al.* Recent climate and ice-sheet changes in West Antarctica compared with the past 2,000 years. *Nature Geoscience* **6**, 372-375, doi:10.1038/ngeo1778 (2013).
- 25 Schneider, D. P. *et al.* Antarctic temperatures over the past two centuries from ice cores. *Geophysical Research Letters* **33**, doi:10.1029/2006gl027057 (2006).
- 26 Mosley-Thompson, E., Thompson, L. G., Grootes, P. M., & Gundestrup, N. Little Ice Age (neoglacial) palaeoenvironmental conditions at Siple Station. *Annals of Glaciology* **14**, 199-204 (1990).
- 27 Mulvaney, R. *et al.* Recent Antarctic Peninsula warming relative to Holocene climate and ice-shelf history. *Nature* **489**, 141-144, doi:10.1038/nature11391 (2012).
- 28 Abram, N. J. *et al.* Acceleration of snow melt in an Antarctic Peninsula ice core during the twentieth century. *Nature Geoscience* **6**, 404-411, doi:10.1038/ngeo1787 (2013).
- 29 Zagorodnov, V. *et al.* Borehole temperatures reveal details of 20th century warming at Bruce Plateau, Antarctic Peninsula. *Cryosphere* **6**, 675-686, doi:10.5194/tc-6-675-2012 (2012).
- 30 Muto, A., Scambos, T. A., Steffen, K., Slater, A. G. & Clow, G. D. Recent surface temperature trends in the interior of East Antarctica from borehole firn temperature measurements and geophysical inverse methods. *Geophysical Research Letters* **38**, doi:10.1029/2011gl048086 (2011).

- 31 Roberts, J. L. *et al.* Borehole temperatures reveal a changed energy budget at Mill Island, East Antarctica, over recent decades. *Cryosphere* **7**, 263-273, doi:10.5194/tc-7-263-2013 (2013).
- 32 Barrett, B. E., Nicholls, K. W., Murray, T., Smith, A. M. & Vaughan, D. G. Rapid recent warming on Rutford Ice Stream, West Antarctica, from borehole thermometry. *Geophysical Research Letters* **36**, doi:10.1029/2008gl036369 (2009).
- 33 Campagne, P. *et al.* Glacial ice and atmospheric forcing on the Mertz Glacier Polynya over the past 250 years. *Nature Communications* **6**, doi:10.1038/ncomms7642 (2015).
- 34 Abram, N. J. *et al.* Ice core evidence for a 20th century decline of sea ice in the Bellingshausen Sea, Antarctica. *Journal of Geophysical Research-Atmospheres* **115**, doi:10.1029/2010jd014644 (2010).
- 35 Curran, M. A. J., van Ommen, T. D., Morgan, V. I., Phillips, K. L. & Palmer, A. S. Ice core evidence for Antarctic sea ice decline since the 1950s. *Science* **302**, 1203-1206, doi:10.1126/science.1087888 (2003).
- 36 Murphy, E. J., Clarke, A., Abram, N. J. & Turner, J. Variability of sea-ice in the northern Weddell Sea during the 20th century. *Journal of Geophysical Research-Oceans* **119**, 4549-4572, doi:10.1002/2013jc009511 (2014).